ResearchGate

See discussions, stats, and author profiles for this publication at: https://www.researchgate.net/publication/247778297

# Ultraviolet–Visible Dual Absorption by Single BODIPY Dye Confined in LTL Zeolite Nanochannels

**ARTICLE** *in* THE JOURNAL OF PHYSICAL CHEMISTRY C · JUNE 2013

Impact Factor: 4.77 · DOI: 10.1021/jp4051676

CITATIONS
10

READS
97

**4 AUTHORS**, INCLUDING:

Hegoi Manzano
Universidad del País Vasco / Euskal Herriko …
**41** PUBLICATIONS **478** CITATIONS
SEE PROFILE

Leire Gartzia-Rivero
Universidad del País Vasco / Euskal Herriko …
**14** PUBLICATIONS **99** CITATIONS
SEE PROFILE

Available from: Hegoi Manzano
Retrieved on: 26 January 2016

THE JOURNAL OF PHYSICAL CHEMISTRY C

Article

pubs.acs.org/JPCC

# Ultraviolet−Visible Dual Absorption by Single BODIPY Dye Confined in LTL Zeolite Nanochannels

Hegoi Manzano,* Leire Gartzia-Rivero, Jorge Bañuelos, and Iñigo López-Arbeloa

Molecular Spectroscopy Laboratory, Department of Physical Chemistry, University of the Basque Country UPV/EHU, Aptdo. 644, 48080-BILBAO, Spain

Supporting Information

**ABSTRACT:** A new hybrid material with dual UV/vis light-harvesting ability has been prepared based on PM546 dye confined in zeolite L nanochannels. Besides the characteristic vis green-yellow absorption of the dye in solution, a new band arises due to specific host−guest interactions, spanning the UV and blue edge of the vis. A chemical reaction takes place between the PM546 and acid protons from the zeolite, removing a fluorine atom from the BODIPY and giving rise to the new hypsochromic absorption. As result, a single dye presents light absorption at two different wavelengths, as well as a broad fluorescence emission, which covers a wide part of the vis region through a FRET process.

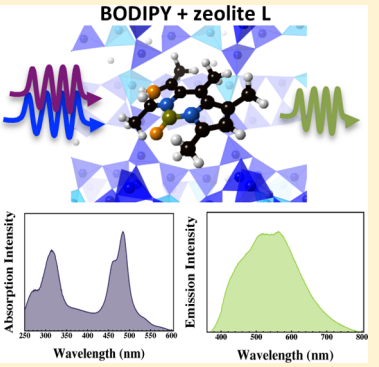


## INTRODUCTION

Hybrid organic inorganic photoelectronic devices are promising alternatives to conventional silicon-based solar cells. They are generally built of cheap and environmentally friendly materials, easily adaptable to operate over a large variety of wavelengths, and can be tailored with versatile designs.[1] The encapsulation of organic fluorophores into a nanostructured host can avoid the formation of aggregates, improve the chemical, thermal, and photochemical stability of the dye, and force it to align in a preferred orientation, crafting highly organized photoactive hybrid materials.[2] Not only the properties of the fluorophores are ameliorated by such a cage effect but also the guest itself may behave as a fluorescent sensor to monitor the properties of the host adsorption sites.[3] Furthermore, the combination of complementary dyes could lead to efficient synergistic effects through an energy transfer process, creating highly adaptable systems. For instance, antenna devices and white-light-emitting systems have been fabricated by the encapsulation inside nanoporous materials of carefully chosen dyes with efficient and tunable Föster resonance energy transfer (FRET).[4]

In this work, we aim to build a hybrid photoactive material for energetic applications, formed by insertion of PM546 into the zeolite L framework (Figure 1). We have chosen such a guest dye, from the boron-dipyrromethene (BODIPY) family, due to its unique photophysical properties.[5,6] Pyrromethenes are characterized by their high fluorescent efficiency, which can be modulated over a wide range of absorption and emission wavelengths, changing the substitution pattern, making them versatile for a wide range of applications.[7] Among the available molecular sieves, zeolite L is a matchless choice.[8−10] Its framework structure results in a series of parallel one-dimensional nanochannels, with a pore aperture of 7 Å.[11] It is ideal to allocate inside fluorophores homogeneously distributed along the zeolite, and strongly oriented in a preferential direction.

We found that the specific interaction between the BODIPY and the zeolite L originates a radical change in the spectral signature of the dye, with the apparition of a new band in the UV-blue region, while conserving the characteristic vis green-yellow absorption. Such an interesting change might be relevant for the application of the system as a light-harvesting material: the nanoconfinement of a single dye in the zeolite can absorb light from two spectral regions far away, increasing the light collection efficiency of the system. Herein, we describe the BODIPY−zeolite L system, characterize its photophysical properties, and investigate the cause of the new spectral band using experimental techniques and atomic-scale simulations.

## EXPERIMENTAL AND THEORETICAL METHODS

**Experimental Methods.** We produced nanosized LTL zeolites with an average size in the largest direction of 45 ± 15 nm via hydrothermal synthesis, using microwave heating to obtain a homogeneous morphology and a narrow size distribution of the crystals. In acidic solutions, the structural integrity of BODIPY is affected, since the protonation of the amine lone pairs lead to the corresponding dipyrromethene by removal of the $BF_2$ bridge.[12−14] To avoid this, we exchanged the zeolitic protons by $Cs^+$ cations,[15] suspending the zeolite L in a saturated solution of CsCl under reflux and stirring during 3 h at 80 °C. The PM546 (laser grade, purchased from

Received: May 25, 2013
Revised: May 31, 2013

 © XXXX American Chemical Society  dx.doi.org/10.1021/jp4051676 | J. Phys. Chem. C XXXX, XXX, XXX−XXX

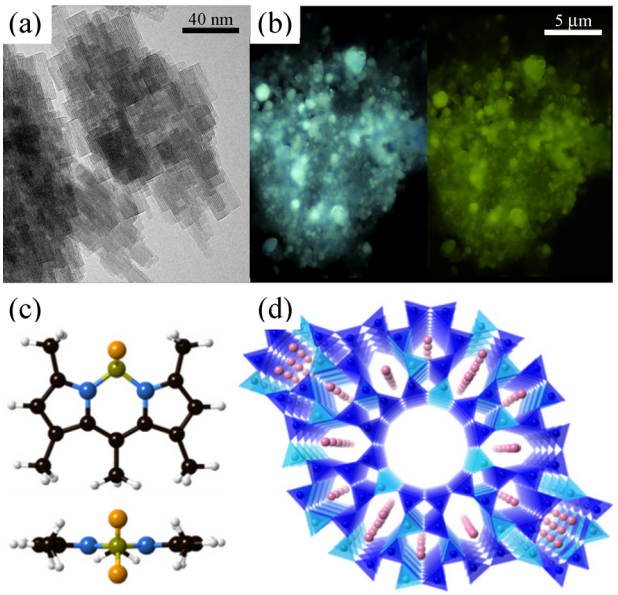


**Figure 1.** (a) TEM image of the nanometric zeolites synthesized using a microwave-assisted hydrothermal method. (b) Fluorescence images of the hybrid zeolite−dye system, under 350/50 and 470/40 nm band-pass excitation and recording the emission with 400 and 515 nm long passes, respectively (from left to right) (c) Atomic representation of the PM546 dye perpendicular and parallel to the molecular plane. The atoms are represented as spheres of several colors: C in black, H in white, N in blue, B in green, and F in orange. (d) Zeolite L supercell representation in the *z* crystallographic direction, perpendicular to the 1D nanochannels. The silicate and aluminate units are represented as dark and light blue tetrahedral omitting the framework oxygen atoms for a better view, and the Cs ions are shown as pink spheres.

Exciton) was then hosted inside the $Cs^+$-exchanged nanozeolite channels by gas-phase adsorption at high temperatures (180° during 2 days). We had previously confirmed the dye stability at the operation temperature, proving that its photophysics did not change after sublimation. Dye-doped zeolite was rinsed with butanol several times.

TEM images were recorded with a Philips CM200 microscope to assign the crystal size (around 45 nm), whereas the crystalinity of the sample was verified by XRD spectra taken in a Bruker D8 Advance Vario.[27] Al-NMR spectra were also recorded before and after dye insertion into the zeolite. The absorption spectra were registered in a Varian spectrophotometer (model Cary 4E) detecting the transmitted light for diluted liquid solutions and the reflected light, by means of an integrating sphere, for the solid samples. The fluorescence steady-state spectra and the CIE 1931 chromaticity diagram were recorded in an Edinburgh Instruments spectrofluorimeter (model FLSP920). The emission measurements were carried out in a right-angle configuration for dye solutions, and in the front-face configuration for dye-doped zeolites (solid state). Fluorescence images were recorded with an optical inverted microscope with an epi configuration (Olympus BX51) equipped with a color CCD (DP72). The excitation was set by Chroma band-pass filters (350/50 and 470/40), and emission was collected with Chroma cutoff filters (E400LPv2 and E515LPv2, from 400 and 515 nm, respectively).

**Computational Methods.** The Monte Carlo code Towhee[16,17] was used to determine the equilibrium position of the cesium ions inside the zeolite in the canonical ensemble.[18] The Cs atoms were initially located close to aluminum. The Monte Carlo movements were then done with a 0.2 Å maximum length for the atomic displacements and an acceptance threshold of 0.5, using the DX-1597-2-7 pseudorandom number generator method.[19] Thermodynamic equilibrium was reached after $10^6$ steps. The potential energy was computed employing the ClayFF force field,[20] using the Edwald summation method account for the long-range electrostatic interactions.[21]

Ab initio molecular dynamics simulations have been carried out within the density functional theory framework[22] with the SIESTA code.[23] A double-ζ polarized basis set was used to represent valence orbitals, with Troullier−Martins pseudopotentials[24] factorized in the Kleiman−Bilander form to mimic the effect of nuclei and core electrons. The calculations were done at the Γ point with a mesh cutoff of 300 Ry. The Born−Oppenheimer dynamics were done in the canonical ensemble, allowing the movement of the guest dye molecule and the host zeolitic framework atoms. We used a 0.1 fs time step to integrate the equation of motion using a Verlet algorithm,[25] and a Nose thermostat[26] coupling constant of 100 Ry $fs^2$. The temperature was increased from 10 to 450 K during 2.5 ps, and then a 25 ps trajectory was simulated: initially 15 ps of the BODIPY inside the Cs-zeolite, and then 10 ps inside the H-zeolite. The structural quantities and energies at the absorption sites were integrated from 5 ps time blocks. Additional MD simulations of the isolated dye were carried out for 10 ps to compare the free and confined conformations of the molecule.

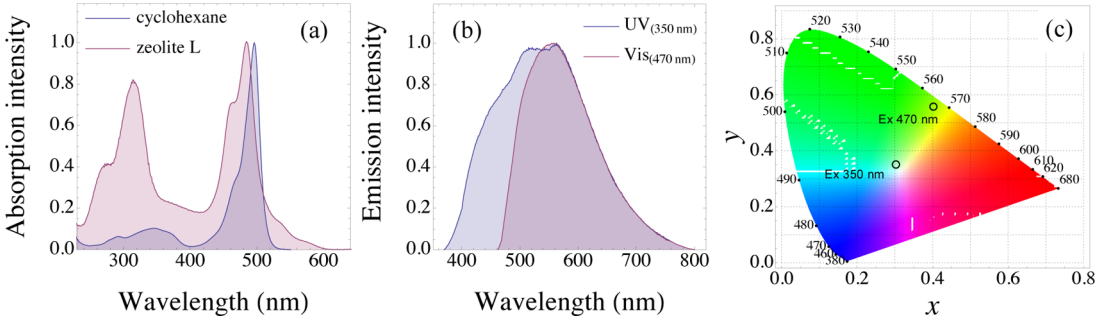


**Figure 2.** (a) Normalized absorption spectra of the PM546 in cyclohexane solution (blue) and confined in the zeolite L nanopores recorded in the solid state (red). The hybrid system preserves the band around 490 nm, and a new signal in the UV region arises. (b) Normalized emission spectra of the BODIPY hosted inside the zeolite collected after excitation at 350 (blue) and 450 nm (red). (c) Representation of the emission colors in the CIE 1931 chromaticity diagram[31] calculated from the fluorescence spectra under 350 and 450 nm irradiation, showing up the white-light emission of the dye-doped material.


dx.doi.org/10.1021/jp4051676 | J. Phys. Chem. C XXXX, XXX, XXX−XXX

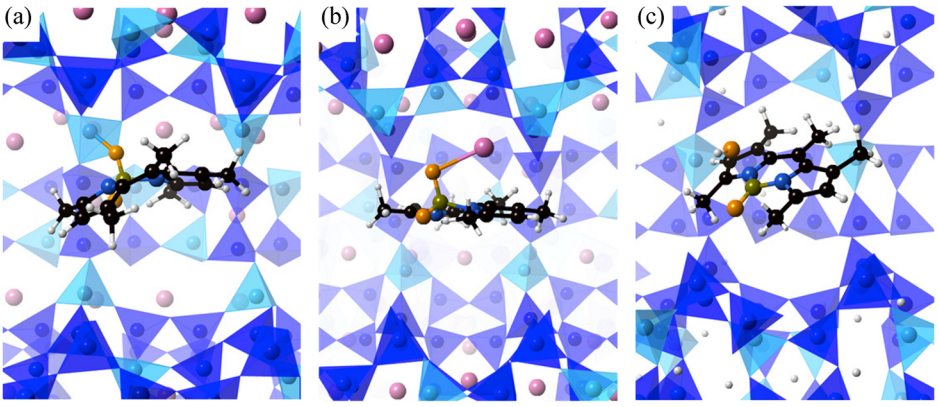


**Figure 3.** Configuration of the dye in the three identified absorption states. The snapshots are taken directly from the MD simulation, and the representation shows the inner part of the zeolitic channels with its longitudinal axis lying horizontally. The color code is the same as that in Figure 1. (a) Al-coordinated absorption site: a fluorine atom from the BODIPY is coordinated to an Al atom from the zeolite. (b) $Cs^+$−BODIPY complex in the zeolite nanochannel. (c) Monofluorated BODIPY $(PM546\text{-}F)^+$ and HF molecules situated in the zeolite channel. The fluorine atom that remains in the dye situates in a planar configuration with the molecule rings.

The electronic structure and absorption spectra were investigated with Gaussian.[27] The molecules obtained from the MD simulations were optimized within the Hartree−Fock theoretical framework, using a LanL2DZ basis set.[28] The absorption spectra were computed considering a Franck−Condon transition in a single-point single-excitation configuration interaction (CIS) calculation,[29] using the same basis set as before.

## RESULTS AND DISCUSSION

The absorption spectrum of the BODIPY confined in the zeolite shows the expected main absorption band at 485 nm, in the middle energetic zone of the visible spectra, which maximum absorption wavelength and shape match with the registered in diluted solutions[5] (Figure 2). Surprisingly, a new band appears at much higher energies and is centered at 315 nm. Such a band has not been previously reported for BODIPY in a wide range of conditions, so we can conclude that the photophysic signature of the dye has changed due to specific interactions with the surrounding environment in the zeolite L channels. The formation of dye aggregates is nevertheless excluded, since the loading was set low enough to avoid it, and the aggregations would lead to absorption bands shifted toward lower energies.

Both absorption processes lead to fluorescent emission. The excitation at 350 nm results in a broad band with a maximum at 545 nm, similar to that recorded after excitation at 450 nm, with the only difference of a hypsochromic shoulder (Figure 2). It is very likely that the new blue fluorescence emission overlaps with the visible absorption band typical of the BODIPY, a Förster resonance energy transfer (FRET) taking place, which explains the single emission. The strong response to polarized light confirms that the dyes are located in the zeolitic channel, most probably as monomers, and indicates that the transition dipole moment (longitudinal molecular axis) of the dyes is disposed coplanar to each other and parallel to the 1D zeolitic channel,[30] factors that enable and maximize FRET processes. The dual light absorption by a single dye over a wide part of the visible and the UV is a very interesting feature for technological applications, such as sensors working in the UV/vis regions. In addition, the broad emission band (white light) enables the emission wavelength modulation (Figure 2), leading to the antenna effect and creating a versatile photoactive system for solar energy harvesting applications.

It is important to understand the origin of the new photophysical process for a future applicability of the developed material. To that end, we carried out an ab initio molecular dynamics simulation of PM546 absorbed in the LTL zeolite with the SIESTA code.[23] We built a 1 × 1 × 3 supercell of all-siliceous LTL zeolite, and substituted randomly Si atoms by Al to achieve the experimental Al/Si ratio of ∼1/3. The charge was balanced by adding Cs ions, optimizing their positions by a Monte Carlo energy minimization process. At equilibrium, the cations are located in the cancrinite and the 8/8-ring intersection cages, but not in the main channels, in agreement with the positions determined by X-ray diffraction.[32] Since our experiments indicate that there is no dye aggregation, a single PM546 molecule was introduced in the main channel, with the larger molecular axis running parallel to the channel direction. We increased the temperature from 10 to 450 K during 2.5 ps, the highest temperature achieved during the incorporation of the dye into the zeolite. Because of the thermal contribution, any chemical process that might affect the BODIPY structural integrity will be more likely in this temperature regime.

During the 25 ps of MD trajectory, we identified two absorption sites (Figure 3a,b). Initially, a fluorine atom from the BODIPY coordinates to an aluminum atom from the zeolitic framework. The chromophore is bonded to the zeolite, and the aluminum coordination changes from tetrahedral to trigonal-bipyramidal. After 5 ps, a cesium cation leaves the cancrinite cages and reaches the main channel. The fluorine atoms of the BODIPY then strongly interact with the electropositive $Cs^+$, leaving the aluminum absorption site. The adsorption energy of the BODIPY forming a $Cs^+$−PM546 complex is 50.9 kcal/mol, 18.1 kcal/mol higher than the Al-coordinated configuration. Therefore, the most favorable thermodynamic configuration of PM546 inside the LTL zeolite corresponds to the dye located in the main channel forming a complex with a cesium counterion. The lower distortion of the dye planarity is the probable reason for the higher stability of this configuration. Furthermore, the identical[27] Al-NMR signal measured for the zeolite before and after the dye insertion indicates that the aluminate units do not change their tetrahedral shape, confirming the absence of this adsorption configuration (see the Supporting Information).


dx.doi.org/10.1021/jp4051676 | J. Phys. Chem. C XXXX, XXX, XXX−XXX

The $Cs^+$−BODIPY complex formation may be the cause of the new absorption band. To address this assumption, we investigated the electronic structure and excitation energies and oscillator strengths of the isolated dye and the cation−dye complex using the Gaussian code.[27] The HOMO−LUMO gap of the $Cs^+$−BODIPY complex is similar to that of the PM546 dye, just 0.001 eV larger. Furthermore, we did not observe any change in the HOMO−LUMO orbitals' spatial representations. Because the electronic structure of both systems is nearly identical, it is not surprising then that they present similar absorption spectra. The shape of the simulated spectra matches qualitatively with the experimental result, yet it is shifted toward higher energies with respect to the experiment due to the CIS overestimation of the energy gap.[33] We can conclude then that the formation of the $Cs^+$−BODIPY complex is not the origin of the new spectral signal in the UV region.

We seek another reason for the new UV absorption band. As mentioned before, the BODIPY dyes are very sensitive to acidic conditions. Although we exchanged the protons with cesium atoms to decrease the acidity of the zeolite, the cationic-exchange efficiency is not 100%.[34] Therefore, we explored the possibility that nonexchanged residual protons of the zeolite cause changes in the dye that explain the new spectral signature. For that end, we replaced the cesium atoms with hydrogen atoms in the final step of the MD trajectory and continued the dynamics. The zeolitic protons migrate from the center of the cancrinite and 8 × 8 intersection cages and coordinate to Si−O−Al bridging oxygen atoms. Regarding the $Cs^+$−dye complex, the substitution of Cs by H entails important structural changes. The strong H−F interaction has a more covalent character than the Cs−F, and the fluorine atom leaves the BODIPY to form hydrogen fluoride, leaving a monofluorated charged dye $(PM546\text{-}F)^+$ (Figure 3c). This reaction is thermodynamically favorable ($\Delta H_{react}$ = −206.7 kcal/mol), and barrier-less since it also takes place during a simple energy minimization process. The simulated absorption spectrum of the $(PM546\text{-}F)^+$ molecule shows the normal band of the BODIPY, together with a new one at higher energies (Figure 4). The shape of the computed spectrum utterly agrees with the experimentally recorded one, so we can conclude that the monofluorated BODIPY is responsible for the UV absorption. From the spatial representation of the molecular orbitals, presented in the Supporting Information, it can be seen that the HOMO and LUMO do not change appreciably after losing a fluorine atom in PM546, and consequently the vis absorption signal is not altered. However, there is a change in the HOMO-2 orbital, responsible for the new UV absorption band. The absence of a fluorine atom changes the spatial distribution of the electrons, increasing the extension of the $\pi$-electron system, and the HOMO-2 to LUMO transition becomes strongly allowed.

The $(PM546\text{-}F)^+$ species explains the experimentally recorded absorption bands. However, the presence of a considerable amount of exchanged $Cs^+$ makes it likely that some dye molecules do not react with protons, and are stabilized in the form of the $Cs^+$−PM546 complex. It is reasonable that both species, the $Cs^+$−PM546 complex and the $(PM546\text{-}F)^+$ molecules, could coexist. Their co-occurrence does not modify the discussed origin of the UV band, and is fully compatible with the experimental spectra. On the one hand, the absorption spectra could be formed by the combination of the UV band that originated from the monofluorated HOMO-2 to LUMO transition and the vis band due to the HOMO to LUMO transition of both species. On the other hand, the emission spectra are similar regardless of the excited band, a fact that we attributed to a Förster resonance energy transfer (FRET) process. In such an energy transfer, the $(PM546\text{-}F)^+$ molecules act as a donor when the UV region is excited, and neighboring $(PM546\text{-}F)^+$ species or $Cs^+$−PM546 complexes could be the acceptor, since both of them present the vis absorption band. It is worth mentioning that the collinear disposition of the molecules in the 1D zeolitic channel maximizes the orientation factor in the Förster formalism.

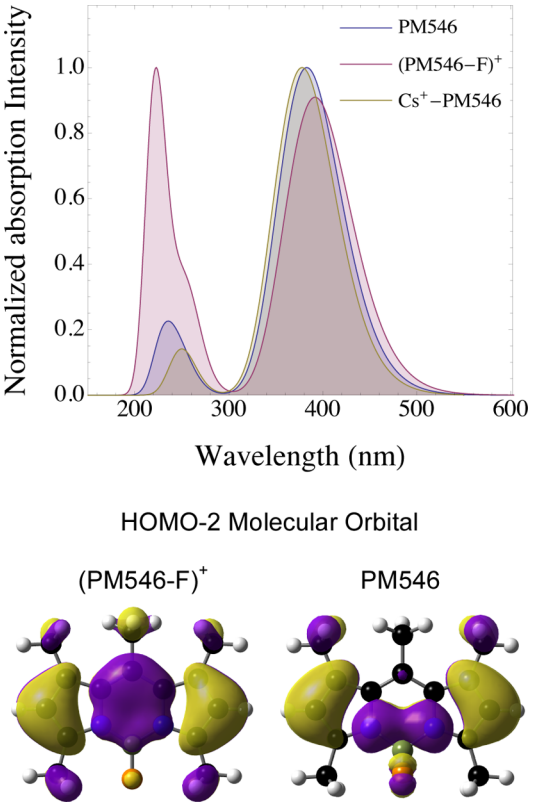


**Figure 4.** (a) Simulated absorption spectra of the P546 dye (blue), the $Cs^+$−PM546 complex (yellow), and the $(PM546\text{-}F)^+$ molecule (red) using the CIS method. There is a clear disparity when a fluorine atom is removed from PM546, since a new band at higher energies that matches the experimental data appears, due to an allowed HOMO-2 to LUMO transition. (b) HOMO-2 molecular orbital representation of the $(PM546\text{-}F)^+$ molecule and the PM546. The higher energy occupied frontier orbitals HOMO and HOMO-1 present the same spatial localization in both systems, as it can be seen in the Supporting Information.

Finally, we investigated another factor that may influence the electronic structure and, therefore, the absorption spectra of the confined BODIPY. According to our simulations, the most stable configuration of PM546 in vacuum is planar, although it can bend considerably due to thermal motion, with a maximum deviation from the planarity of ±21°. When the dye is confined in the zeolitic channel, there is a geometrical constrain that forces the BODIPY to bend, and the equilibrium angle departs considerably from the planarity. In section 2 of the Supporting Information, we present the equilibrium angles of the dye averaged over 5 ps of the molecular dynamics trajectory. It can be seen that the $(PM546\text{-}F)^+$ and $Cs^+$−PM546 species have equilibrium angles of 19.9° and 13.7°, respectively. In addition,


dx.doi.org/10.1021/jp4051676 | J. Phys. Chem. C XXXX, XXX, XXX−XXX

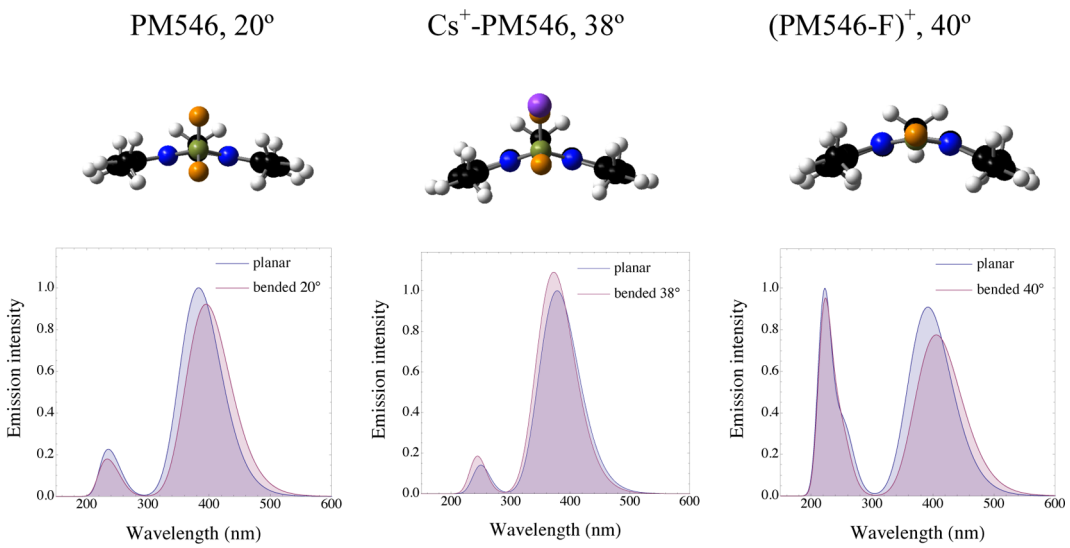


**Figure 5.** Simulated absorption spectra of the PM546, $Cs^+$−PM546, and $(PM546\text{-}F)^+$ species in their planar equilibrium configurations and at the maximum bending angle recorded during the molecular dynamics trajectory.

the thermal motion induces further bending, with a maximum deviation of ±20°, similar to that of the free dye.

Such a distortion from planarity might reduce the delocalization of the orbitals across the dye, decreasing their absorption intensity or inducing spectral shifts. To study this possibility, we computed the absorption spectra of the three species, PM546, $(PM546\text{-}F)^+$, and $Cs^+$−PM546, at the maximum recorded deviation from planarity (21, 40, and 38°, respectively). First, we fixed the dihedral angle at the desired value, and relaxed the remaining atomic positions. A single-point CIS calculation was then performed to the optimized structure. The results are presented in Figure 5. The spectra of the bent configurations have been normalized with respect to the maxima of the planar configurations to have an indication of the changes in the oscillator strength. The results reveal that the distortion does not affect substantially the absorption spectra. There are small changes in the oscillator strength and small displacement of the absorption maxima, although none of the changes are important.

## CONCLUSIONS

In this work, we have presented a new hybrid photoactive material, based on the confinement of PM546 dyes into nanometric channels of the LTL zeolite. The hybrid system presents light absorption covering a wide part of the UV−vis regions. Such a spectral signature makes the material very versatile, since a single material could harvest light from two spectral regions far from each other. The new UV absorption band originated from a chemical change of the BODIPY. Fluorine atoms from the dye react with protons of the zeolitic framework, and one F atom leaves the dye. The newly found molecule preserves the HOMO−LUMO structure of the PM546, while the electronic structure of the HOMO-2 changes, making the HOMO-2 to LUMO transition strongly allowed. This fact is remarkable, since other dyes hosted in zeolites do not preserve the band characteristic of basic pH after protonation.[35]

Regardless of the excited band, a fluorescent emission with a similar wavelength is achieved via FRET-type energy transfer. This simplifies and enhances the light-harvesting process, collecting energy at different wavelengths simultaneously with just one fluorophore, and makes the system appealing for the development of antenna devices. Further effort is being carried out to tune the absorption and emission of the presented hybrid system, modifying the substitution pattern of the BODIPY. It is worth mentioning that the high sensitivity of PM546 to protons makes it a possible candidate as acidity site sensors in zeolites.

## ASSOCIATED CONTENT

### Supporting Information

X-ray diffraction pattern of the synthesized nanozeolite; structural data of the PM546 in vacuum, the PM546 coordinated to zeolitic Al, the $Cs^+$−PM546 complex inside the zeolite, and the $(PM546\text{-}F)^+$ species inside the zeolite; $^{27}$Al-NMR of the zeolite with and without dye loading, and structural data of the aluminum coordinated to the PM546; spatial representation of the HOMO-2, HOMO-1, HOMO, and LUMO orbitals of all the molecules; and wavelengths and oscillator strengths of the HOMO-2 to LUMO, HOMO-1 to LUMO, and HOMO to LUMO transitions. This material is available free of charge via the Internet at http://pubs.acs.org.

## AUTHOR INFORMATION

### Corresponding Author

*E-mail: hegoi.manzano@ehu.es.

### Notes

The authors declare no competing financial interest.

## ACKNOWLEDGMENTS

This work was supported by the Spanish Government through the MAT2010-20646-204-04 project. H.M. and L.G.-R. acknowledge, respectively, the IT339-10 contract and the Ph.D. grant from the Basque Country Department of Education, Research, and Universities. The computing resources, transmission electron microscopy (TEM), X-ray diffraction (XRD), and aluminum nuclear magnetic resonance ($^{27}$Al-NMR) measurements of the SGIker (UPV/EHU) are gratefully acknowledged, as well as the computing resources of the i2Basque project.

## REFERENCES


(1) Mech, A.; Monguzzi, A.; Meinardi, F.; Mezyk, J.; Macchi, G.; Tubino, R. Sensitized NIR Erbium(III) Emission in Confined Geometries: A New Strategy for Light Emitters in Telecom Applications. *J. Am. Chem. Soc.* **2010**, *132* (13), 4574−4576.

(2) Calzaferri, G. Nanochannels: Hosts for the Supramolecular Organization of Molecules and Complexes. *Langmuir* **2012**, *28* (15), 6216−6231.

(3) Corma, A.; Díaz, U.; García, T.; Sastre, G.; Velty, A. Multifunctional Hybrid Organic−Inorganic Catalytic Materials with a Hierarchical System of Well-Defined Micro- and Mesopores. *J. Am. Chem. Soc.* **2010**, *132* (42), 15011−15021.

(4) Ramachandra, S.; Schuermann, K. C.; Cucinotta, F.; Calzaferri, G.; De Cola, L. Förster Resonance Energy Transfer in Quantum Dot Dye Loaded Zeolite L Nanoassemblies. *Small* **2011**, *7* (10), 1488−1494.

(5) López-Arbeloa, F.; Bañuelos, J.; Martinez, V.; Arbeloa, T.; López-Arbeloa, I. Structural, Photophysical and Lasing Properties of Pyrromethene Dyes. *Int. Rev. Phys. Chem.* **2005**, *24* (2), 339−374.

(6) Ulrich, G.; Ziessel, R.; Harriman, A. The Chemistry of Fluorescent Bodipy Dyes: Versatility Unsurpassed. *Angew. Chem., Int. Ed.* **2008**, *47* (7), 1184−1201.

(7) Loudet, A.; Burgess, K. BODIPY Dyes and Their Derivatives: Syntheses and Spectroscopic Properties. *Chem. Rev.* **2007**, *107* (11), 4891−4932.

(8) Cheetham, A. K.; Férey, G.; Loiseau, T. Open-Framework Inorganic Materials. *Angew. Chem., Int. Ed.* **1999**, *38* (22), 3268−3292.

(9) Tao, Y.; Kanoh, H.; Abrams, L.; Kaneko, K. Mesopore-Modified Zeolites: Preparation, Characterization, and Applications. *Chem. Rev.* **2006**, *106* (3), 896−910.

(10) Schulz-Ekloff, G.; Wohrle, D.; van Duffel, B.; Schoonheydt, R. A. Chromophores in Porous Silicas and Minerals: Preparation and Optical Properties. *Microporous Mesoporous Mater.* **2002**, *51* (2), 91−138.

(11) Barrer, R.; Villiger, H. The Crystal Structure of the Synthetic Zeolite L. *Z. Kristallogr.* **1969**, *128* (3−6), 352−370.

(12) Reisfeld, R.; Yariv, E.; Minti, H. New Developments in Solid State Lasers. *Opt. Mater.* **1997**, *8* (1), 31−36.

(13) Bañuelos, J.; López Arbeloa, F.; Arbeloa, T.; Salleres, S.; Vilas, J.; Amat-Guerri, F.; Liras, M.; López Arbeloa, I. Photophysical Characterization of New 3-Amino and 3-Acetamido BODIPY Dyes with Solvent Sensitive Properties. *J. Fluoresc.* **2008**, *18* (5), 899−907.

(14) Li, J.; Hu, B.; Hu, G.; Li, X.; Lu, P.; Wang, Y. An Efficient Synthesis of Heptaaryldipyrromethenes from Tetraarylcyclopentadienones and Ammonium Acetate and Their Extension to the Corresponding BODIPYs. *Org. Biomol. Chem.* **2012**, *10* (44), 8848−8859.

(15) Albuquerque, R. Q.; Calzaferri, G. Proton Activity inside the Channels of Zeolite L. *Chem.—Eur. J.* **2007**, *13* (32), 8939−8952.

(16) Martin, M. G. *MCCS Towhee 7.0.2*; 2012. http://towhee.sourceforge.net.

(17) Martin, M. G.; Thompson, A. P. Industrial Property Prediction Using Towhee and Lammps. *Fluid Phase Equilib.* **2004**, *217* (1), 105−110.

(18) Metropolis, N.; Rosenbluth, A. W.; Rosenbluth, M. N.; Teller, A. H.; Teller, E. Equations of State Calculations by Fast Computing Machines. *J. Chem. Phys.* **1953**, *21* (6), 1087−1092.

(19) Deng, L.-Y. Efficient and Portable Multiple Recursive Generators of Large Order. *ACM Trans. Model. Comput. Simul. (TOMACS)* **2005**, *15* (1), 1−13.

(20) Cygan, R. T.; Liang, J. J.; Kalinichev, A. G. Molecular Models of Hydroxide, Oxyhydroxide, and Clay Phases and the Development of a General Force Field. *J. Phys. Chem. B* **2004**, *108* (4), 1255−1266.

(21) Ewald, P. P. The Calculation of Optical and Electrostatic Grid Potential. *Ann. Phys.* **1921**, *64* (3), 253−287.

(22) Parr, R. G.; Yang, W. *Density-Functional Theory of Atoms and Molecules*; Oxford University Press: Oxford, England, 1989.

(23) Artacho, E.; Anglada, E.; Dieguez, O.; Gale, J. D.; Garcia, A.; Junquera, J.; Martin, R. M.; Ordejon, P.; Pruneda, J. M.; Sanchez-Portal, D.; Soler, J. M. The Siesta Method; Developments and Applicability. *J. Phys.: Condens. Matter* **2008**, *20* (6), 064208.

(24) Troullier, N.; Martins, J. L. Efficient Pseudopotentials for Plane-Wave Calculations. *Phys. Rev. B* **1991**, *43* (3), 1993−2006.

(25) Verlet, L. Computer Experiments on Classical Fluids. I. Thermodynamical Properties of Lennard-Jones Molecules. *Phys. Rev.* **1967**, *159* (1), 98.

(26) Nose, S. A Molecular Dynamics Method for Simulations in the Canonical Ensemble. *Mol. Phys.* **1984**, *52* (2), 255−268.

(27) Frisch, M. J.; Trucks, G. W.; Schlegel, H. B.; Scuseria, G. E.; Robb, M. A.; Cheeseman, J. R.; Montgomery, J. A., Jr.; Vreven, J. T.; Kudin, K. N.; Burant, J. C.; Millam, J. M.; Iyengar, S. S.; Tomasi, J.; Barone, V.; Mennucci, B.; Cossi, M.; Scalmani, G.; Rega, N.; Petersson, G. A.; Nakatsuji, H.; Hada, M.; Ehara, M.; Toyota, K.; Fukuda, R.; Hasegawa, J.; Ishida, M.; Nakajima, T.; Honda, Y.; Kitao, O.; Nakai, H. M. X.; Hratchian, E. P.; Cross, J. B.; Adamo, C.; Jaramillo, J.; Gomperts, R.; Stratmann, R. E.; Yazyev, O.; Austin, A. J.; Cammi, R.; Pomelli, C.; Ochterski, J. W.; Ayala, P. Y.; Morokuma, K.; Voth, G. A.; Salvador, P.; Dannenberg, J. J.; Zakrzewski, V. G.; Dapprich, S.; Daniels, A. D.; Strain, M. C.; Farkas, O.; Malick, D. K.; Rabuck, A. D.; Raghavachari, K.; Foresman, J. B.; Ortiz, J. V.; Cui, Q.; Baboul, A. G.; Clifford, S.; Cioslowski, J.; Stefanov, B. B.; Liu, G.; Liashenko, A.; Piskorz, P.; Komaromi, I.; Martin, R. L.; Fox, D. J.; Keith, T.; Al-Laham, M. A.; Peng, C. Y.; Nanayakkara, A.; Challacombe, M.; Gill, P. M. W.; Johnson, B.; Chen, W.; Wong, M. W.; Gonzalez, C.; Pople, J. A. *Gaussian 03*, Revision B.04; Gaussian Inc.: Pittsburgh, PA, 2003.

(28) Wadt, W. R.; Hay, P. J. Ab Initio Effective Core Potentials for Molecular Calculations. Potentials for Main Group Elements Na to Bi. *J. Chem. Phys.* **1985**, *82* (1), 284.

(29) Foresman, J. B.; Head-Gordon, M.; Pople, J. A.; Frisch, M. J. Toward a Systematic Molecular Orbital Theory for Excited States. *J. Phys. Chem.* **1992**, *96* (1), 135−149.

(30) Gartzia-Rivero, L.; Bañuelos-Prieto, J.; Martínez-Martínez, V.; López-Arbeloa, I. Versatile Photoactive Materials Based on Zeolite L Doped with Laser Dyes. *ChemPlusChem* **2012**, *77* (1), 61−70.

(31) Smith, T.; Guild, J. The C.I.E. Colorimetric Standards and Their Use. *Trans. Opt. Soc.* **1931**, *33* (3), 73.

(32) Seoung, D.; Lee, Y.; Kim, S. J.; Lee, H.-H.; Ahn, D.; Shin, N.-S.; Vogt, T.; Lee, Y. Pressure-Induced Hydration and Cation Migration in a $Cs^+$ Exchanged Gallosilicate Zeolite LTL: Synchrotron X-Ray Powder Diffraction Study at Ambient and High Pressures. *Microporous Mesoporous Mater.* **2010**, *136* (1−3), 75−82.

(33) Cramer, C. J. *Essentials of Computational Chemistry: Theories and Models*; John Wiley & Sons: Chichester, England, 2002.

(34) Calzaferri, G.; Leiggener, C.; Glaus, S.; Schurch, D.; Kuge, K. i. The Electronic Structure of $Cu^+$, $Ag^+$, and $Au^+$ Zeolites. *Chem. Soc. Rev.* **2003**, *32* (1), 29−37.

(35) Bussemer, B.; Dreiling, I.; Grummt, U.-W.; Mohr, G. J. Spectroscopic and Quantum Chemical Study of the Brønsted Acid Sites in Zeolite L Channels with Acidochromic Cyanine Dyes. *J. Photochem. Photobiol., A* **2009**, *204* (2), 90−96.